Cryogenics 104 (2019) 102992

Contents lists available at ScienceDirect

Cryogenics

journal homepage: www.elsevier.com/locate/cryogenics

Thermal structure optimization of a supercondcuting cavity vertical test cryostat

Shufeng Jin[a,b], Shuping Chen[a,*], Rongzhen Zhao[b,*], Junhui Zhang[c], Hailin Su[c]

[a] College of Petrochemical Engineering, Lanzhou University of Technology, Lanzhou 730050, People's Republic of China
[b] School of Mechanical and Electrical Engineering, Lanzhou University of Technology, Lanzhou 730050, People's Republic of China
[c] Institute of Modern Physics, Chinese Academy of Sciences, Lanzhou 730050, People's Republic of China

ARTICLE INFO

Keywords:
Superconducting vertical test
Cryostat
Heat transfer
Thermal intercept
Experiment

ABSTRACT

The cryostat for superconducting cavity vertical tests (SCVT) studied in this paper has the following two characteristics. One is that there is an uninsulated part of the inner vessel, which is exposed to the environment, to heat the outflow gas to prevent frost formation, and another is that there is a vapor cooled screen in direct contact with the inner vessel forming a thermal intercept. Based on the above characteristics, a heat leakage model for the SCVT cryostat was established in the case where the evaporation gas is involved. The effects of the thermal intercept position, height of the uninsulated part of the inner vessel and liquid level height on the heat leakage and gas outlet temperature of the cryostat were studied. The results showed that the thermal intercept position at 0.34 times the height of the insulation part of the inner vessel has the minimum required power, and at 0.388 times the height has the minimum heat leakage. The optimal thermal intercept position considering required power and heat leakage is located at 0.376 times the height of the insulated part. As the height of the uninsulated part changes from 0.1 m to 0.6 m, the gas outlet temperature rises from 71.83 K to 290 K. Although the heat leakage increases greatly with the height of the uninsulated part rises, it is mainly used to heat the outflow gas, which has less influence on the liquid helium evaporation. With a liquid level height from 1.8 m to 2.4 m, the gas outlet temperature has decreased by 29.6 K, and the heat leakage increases by 1.69%. The heat leakage and gas outlet temperature is not sensitive to the liquid level height.

1. Introduction

In recent years, superconducting cavity technology has maintained improving rapidly, injecting vitality into accelerator development by its excellent performance [1]. In order to guarantee the accelerator gradient and Q value of the superconducting cavity, the cryogenic performances of the cavity need to be measured by vertical tests before operation. The cryostat of the superconducting cavity vertical tests (SCVT), which is used to store the liquid helium needed to surround the cavity, is one of the key equipment for the cryogenic performance measurement [2,3], as shown in Fig. 1. The SCVT cryostat is composed of an inner and an outer vessel is a large neck cryogenic vessel. The liquid helium in the cryostat is easy to evaporate under heat load, resulting in energy waste. Therefore, the thermal insulation of the cryostat using the composite insulation of high vacuum multilayer and a vapor cooled screen is particularly important. The vapor cooled screen is in direct contact with the inner vessel, and forms a thermal intercept between the environment temperature of 300 K and the liquid helium temperature of 4.2 K. The thermal intercept is beneficial to reduce the heat leakage of the cryostat. Meanwhile, in order to prevent the cryostat from frosting, the thermal insulation does not completely enclose the inner vessel to obtain high outlet gas temperature. In other words, an uninsulated part of the inner vessel is exposed to the environment, causing an increase in heat leakage. In view of the minimum heat leakage and anti-frosting, it is necessary to analyse the influence of the thermal structure on the heat leakage of the cryostat.

As an indispensable part of the cryogenic vessel, the thermal insulation has been studied by many experimental and theoretical investigations. The heat leakage of the cryogenic vessel was calculated theoretically by Wang [4], and the results were validated by using liquid nitrogen as working medium. The comparison showed that the error was small. A layer-by-layer heat transfer model was developed to numerically calculate heat transfer of the high vacuum multilayer insulation (HV-MLI) [5,6]. As compared with experiment result, the

* Corresponding authors.
E-mail addresses: jinshufeng100@163.com (S. Jin), chensp@lut.cn (S. Chen), zhaorongzhen@lut.cn (R. Zhao), junhui_zh@impcas.ac.cn (J. Zhang), suhl@impcas.ac.cn (H. Su).

https://doi.org/10.1016/j.cryogenics.2019.102992
Received 17 February 2019; Received in revised form 18 October 2019; Accepted 22 October 2019
Available online 24 October 2019

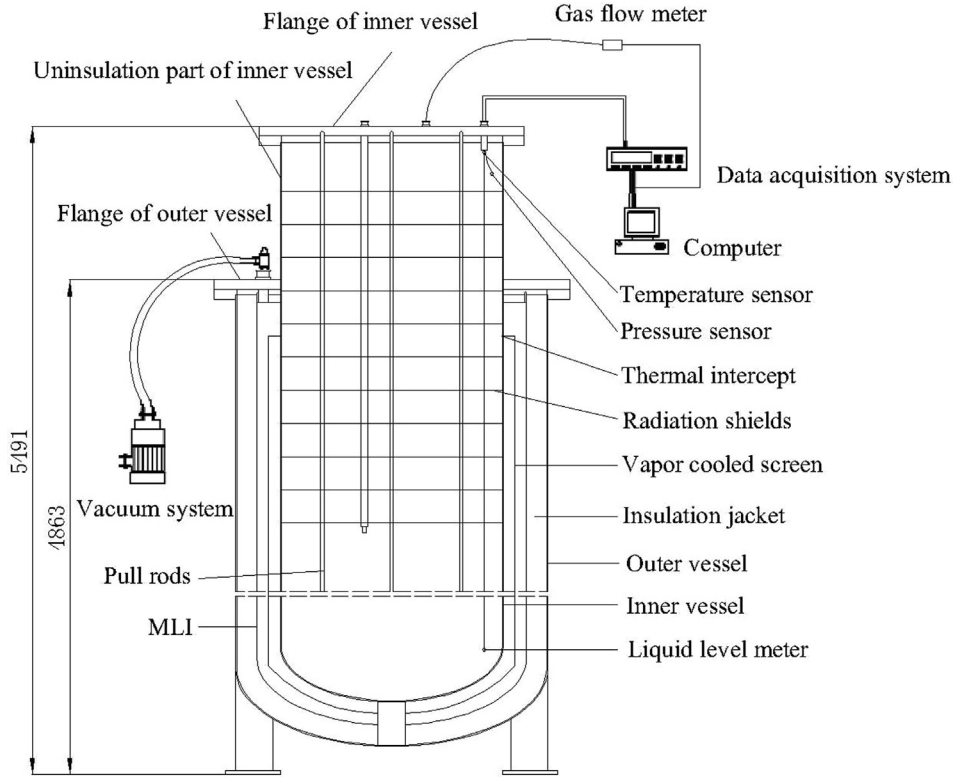

Fig. 1. Schematic diagram of experimental setup.

deviation of the calculated thermal conductivity is within 30% [5]. A method for optimizing the configuration of variable density multilayer insulation (VD-MLI) has been proposed by Wang [7]. They found that the performance of the optimized VD-MLI is improved by 45.5% compared to uniform density multilayer insulation, and dacron net spacers help the VD-MLI further improve the insulation performance by over 50%. A combination of foam and VD-MLI for cryogen storage was investigated by experiment and numerical method [8,9]. The temperature profile and mean heat flux of foam and multilayer insulation (MLI) samples were measured at different vacuum level, and the measured heat flux of VD-MLI was lower than that of MLI by 17.49%. The influence and optimization of the getter on the thermal insulation property of the HV-MLI were studied [10,11]. The results showed that CuO & C was suitable to adsorb H_2 in HV-MLI tank, and the addition of C enables CuO to absorb H_2. The adsorption rate is increased by one order of magnitude with the addition of Cu. The insulation performance of MLI doped with phase change material was analyzed by Xie [12]. The best arrangement of MLI material to achieve optimum insulation performance was found. The composite of HV-MLI and vapor cooled shield was explorated and optimized [13,14]. It turned that the optimal position of vapor cooled shield locates at the middle of the VD-MLI's thickness. Wang [15] established a theoretical calculation model for the heat leakage of the SCVT cryostat, and verified it with liquid nitrogen and liquid helium. The main heat leakage parts were determined and the improvement plan was put forward.

Unfortunately, there are few studies on the thermal structure of the cryostat used in the SCVT. Many scholars focus on the system of the SCVT cryostat, such as the systematic design [16], diagnostic system [17], magnetic shielding [18] and so on. Moreover, the previous researches on the heat leakage of cryogenic vessel have ignored the effects of evaporation gas and thermal intercept formed by the vapor cooled screen. In this present study, a theoretical heat leakage model of the SCVT cryostat was established in the case where the gas is involved in heat leakage, and the rationality of the model was verified by experiment. According to the principle of minimum heat leakage and antifrosting, an optimization of the thermal intercept position was carried out. The influences of the height of the uninsulated part of the inner vessel and liquid level height of helium on gas outlet temperature and heat leakage were evaluated in detail.

2. Experimental setup

The schematic diagram of the experimental setup is shown in Fig. 1. The experimental system is based on the SCVT system and works simultaneously with the cryogenic performance measurement of superconducting cavity. It consists of four main parts: cryostat, insulation jacket, vacuum system and data acquisition system.

The cryostat is a large neck cryogenic vessel composed of inner and outer vessels. The inner vessel contains two parts: an uninsulated part and an insulated part. In order to reduce the radiation heat leakage of the flange of the inner vessel, the radiation shields fixed by the pull rods are applied. The materials and dimensions of inner vessel, outer vessel, and radiation shields are shown in Table 1.

The inner vessel uses a composite insulation of HV-MLI and a vapor cooled screen. The HV-MLI consists of reflectors and spacers. The reflectors are aluminum foil, and the spacers are nylon cloth. The total number of reflectors and spacers is 40 layers with the thickness of 30 mm. The vapor cooled screen is made of a copper screen welded with

Table 1
Materials and dimensions of the parts.

	Material	Dimension		
		Diameter (mm)	Thickness (mm)	Length (mm)
Inner vessel	316L stainless steel	Φ800	3	5107
Outer vessel	316L stainless steel	Φ1120	8	4652
Radiation shields	Polyurethane board with two-sided aluminizing	Φ780	2	11-Layer

spiral tube, and is riveted on inner vessel. Argon arc welding is adopted between copper screen and spiral tube. The vapor cooled shield is placed in the middle of the HV-MLI. The distance from the top of the vapor cooled screen to the flange of the outer vessel is 700 mm. The cooling medium used in the vapor cooled screen is liquid nitrogen.

The vacuum system was continuously operated during the experiment to maintain the vacuum level of 10^{-3} Pa. The data acquisition system includes temperature sensor, pressure sensor, gas flow meter, liquid level meter and data acquisition. Before the experiment started, nitrogen gas was first used to purge the cryostat, and then the whole system was pre-cooled to 77 K by liquid nitrogen which was discharged finally. Afterwards, helium gas was used to further cooldown, and in the end the test temperature was reached at 4.2 K through liquid helium cooling. After the cryostat has been sufficiently stable, the experiment data were record. During the experiment, the liquid helium was continuously injected to make its height meet the test requirements. The effective liquid level height of the inner vessel is 2100 mm.

3. Heat leakage model

Consistent with the experiment, the heat leakage of the cryostat under the steady state condition is analyzed. The cryostat structure studied in this paper is different from the common cryogenic vessel, and the uninsulated part of the inner vessel is exposed to the environment. The heat leakage model of the cryostat is shown in Fig. 2. Different from previous studies, this model takes into account the heat transfer of evaporation gas. Due to the influence of radiation shields, the heat transfer of evaporation gas can be divided into two parts as shown in Fig. 2(b). One part is coupling heat transfer with the radiation shields (the area bounded by dotted line in Fig. 2(b)), and the other part is convection heat transfer with the wall of the inner vessel. In addition, the heat leakages of pipelines and support are small and not considered. So the heat leakage mainly contain four parts: heat transfer (Q_1) of the radiation shields, heat conduction (Q_2) from environment to liquid helium through the inner vessel wall in the axial, convection heat transfer (Q_3) between the environment and the uninsulated part of the inner vessel, and comprehensive heat transfer (Q_4) through the insulation jacketed. At steady state condition, all the heat leakage to the cryostat is absorbed by the evaporated gas and liquid helium. So the heat balance equation can be written as

$$Q = Q_1 + Q_2 + Q_3 + Q_4 = \dot{m}(r + c_p(T_G - T_H)) \tag{1}$$

where Q is heat leakage to the cryostat, $\dot{m}$ is the mass flow rate of evaporation gas, T_G is the outlet temperature of evaporation gas, T_H is the temperature of liquid helium, r is the latent heat of liquid helium, and c_p is the specific heat of evaporation gas.

Based on layer-by-layer heat transfer model, the coupling heat transfer between the evaporation gas and the radiation shields has been researched by the author in another article [19]. The research has obtained the heat transfer rate Q_1 which is expressed as

$$Q_1 = 11.94A_1 \tag{2}$$

where A_1 is the radiation shield area.

As shown in Fig. 2(a), the connection position between the outer vessel flange and the inner vessel is defined as position a, position b represents the contact point between the vapor cooled screen and the inner vessel, and position c is the liquid level. Due to the influence of these positions, there is a thermal intercept along the inner vessel wall. So the heat transfer rate Q_2 from the environment to the liquid helium through the inner vessel wall in the axial is calculated as

$$Q_2 = -A_2 \frac{1}{x_c - x_b} \int_{T_b}^{T_c} \lambda_s(T)dT \tag{3}$$

where A_2 is the cross-sectional area of the inner vessel, T is the temperature of the inner vessel wall, T_b and T_c are temperatures of position b and position c respectively, x_b and x_c are distances of position b and position c in the x direction in the Cartesian coordinate system as shown in Fig. 2(a) respectively, and λ_s is the thermal conductivity of the inner vessel. The relationship of λ_s with temperature is as follows

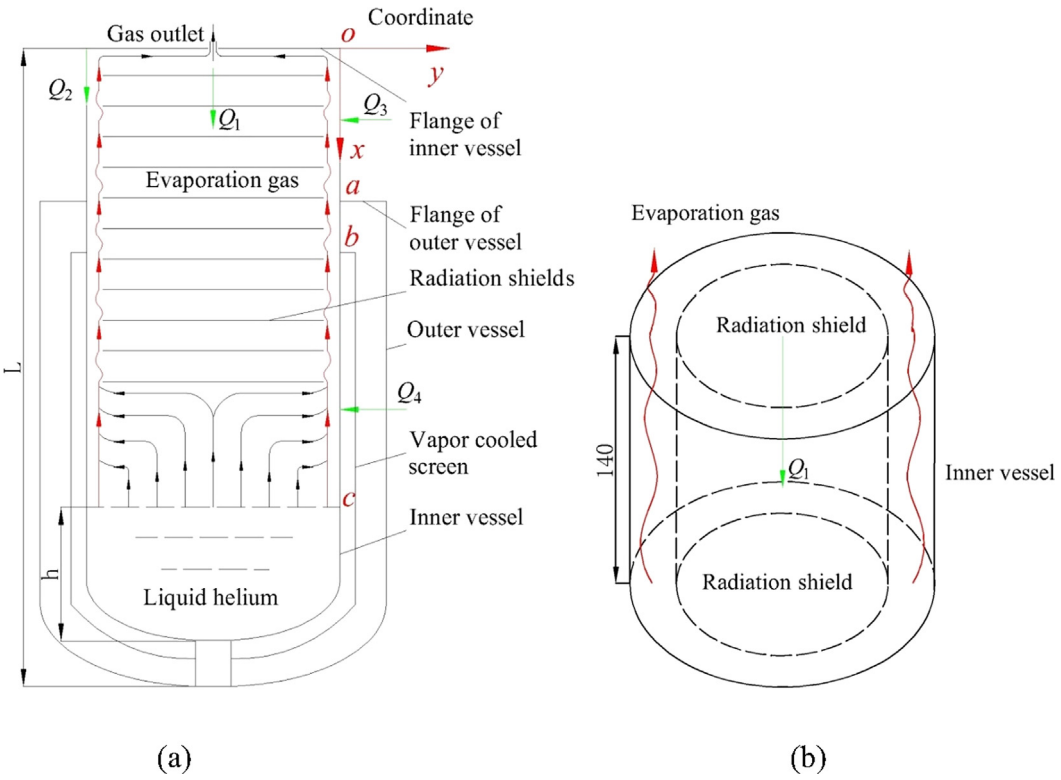

Fig. 2. Heat leakage transfer model.

$$\lambda_s(T) = -2.8135 \times 10^{-9}T^4 + 2.6387 \times 10^{-6}T^3 - 9.1933 \times 10^{-4}T^2 + 0.1678T - 0.7344 \quad (4)$$

The heat transfer rate Q_3 between the environment and the uninsulated part of the inner vessel can be written as

$$Q_3 = A_3 \int_{x_0}^{x_a} h(T_0 - T(x))dx \quad (5)$$

where A_3 is the superficial area of the uninsulated part of the inner vessel, T_o is environment temperature, x_a is distances of the position a, and h is natural convective heat transfer coefficient outside the cylinder. The expression of h can be defined as

$$h = 0.59(Gr\ \ Pr)^{1/4} \quad (6)$$

where Gr and Pr are Grachef and Prandtl numbers of the air, respectively.

According to positions of the liquid level and the vapor cooled screen, the heat transfer rate Q_4 through the insulation jacketed is divided into three segments: $x_a \rightarrow x_b$, $x_b \rightarrow x_c$, and h. It can be obtained by

$$Q_4 = \frac{2\pi\lambda_i(x_b - x_a)}{\ln(r_3/r_1)} \int_{x_a}^{x_b} (T_o - T(x))dx + \frac{2\pi\lambda_i(x_c - x_b)}{\ln(r_2/r_1)} \int_{x_b}^{x_c} (T_b - T(x))dx + \frac{2\pi\lambda_i h}{\ln(r_2/r_1)}(T_b - T_c) \quad (7)$$

where r_1, r_2, and r_3 are the radius of inner vessel, vapor cooled screen and HV-MLI respectively, and λ_i is apparent thermal conductivity of the HV-MLI.

4. Results and discussion

4.1. Axial temperature field of inner vessel wall

From Eqs. (3), (5) and (7), it is known that the axial temperature field of the inner vessel wall is required to calculate the heat leakage. As shown in Fig. 2(a), the temperature field can be divided into three segments: position o to position a, position a to position b, and position b to position c. Because the wall thickness of the inner vessel is far less than the height, according to the one-dimensional steady-state thermal conductivity differential equation ($d^2T/dx^2 = 0$), the temperature is considered to be linearly distributed in each segment, and can be written as

$$T(x) = C_1x + C_2 \quad (8)$$

The initial conditions for the segment of position o to position a is

$$\begin{cases} x = x_o = 0 \\ T = T_o = 300 \end{cases} \quad \begin{cases} x = x_a = 0.5 \\ T = T_a = 282 \end{cases} \quad (9)$$

for position b to position c is

$$\begin{cases} x = x_a = 0.5 \\ T = T_a = 282 \end{cases} \quad \begin{cases} x = x_b = 1.2 \\ T = T_b = 80 \end{cases} \quad (10)$$

and for position c to position d is

$$\begin{cases} x = x_b = 1.2 \\ T = T_b = 80 \end{cases} \quad \begin{cases} x = x_c = 3 \\ T = T_c = 4.2 \end{cases} \quad (11)$$

The axial temperature field of the inner vessel wall is as follows

$$T(x) = \begin{cases} -36x + 300 & o \rightarrow a \\ -288.57x + 426.29 & a \rightarrow b \\ -41.94x + 130.33 & b \rightarrow c \end{cases} \quad (12)$$

Fig. 3 shows the variation of the inner vessel wall temperature with the distance in the axial direction.

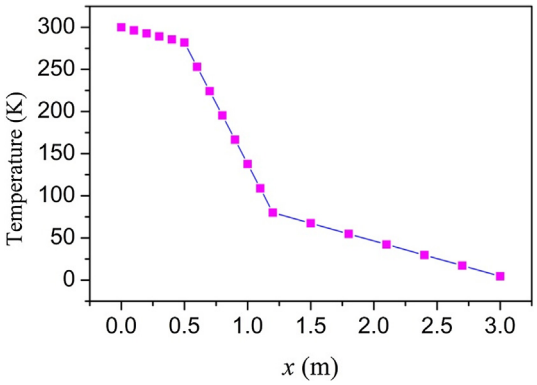

Fig. 3. Axial temperature distribution of the inner vessel wall.

4.2. Heat transfer rate

The relevant data used to calculate the heat leakage measured by the experiment are shown in Table 2. These data and Eq. (12) are substituted into the heat leakage model to obtain the heat leakage of the cryostat to be 41.45 W. The heat leakage obtained by the experiment is 45.05 W, and the error with the model calculation result is 8%. The reason for the error is that the model calculation did not take into account the heat leakage of pipelines, supports and electrical components. So the heat leakage model established above can be considered feasible. The heat leakage and the proportion of each part are shown in Fig. 4. It can clearly be seen that the heat transfers through the uninsulated part of the inner vessel and the jacket account for the main part of the heat leakage. The heat transfer rate between the environment and the uninsulated part of the inner vessel has the highest proportion of 50.3%, the heat transfer rate through the insulation jacket has the second highest proportion of 32.4%, and the heat transfer rate from the environment to the liquid helium has the smallest proportion of 3.5%.

4.3. Thermal intercept position

The vapor cooled screen is in direct contact with the outer wall of the inner vessel, and forms a thermal intercept in the axial heat conduction of the inner vessel. Similarly, there is a thermal intercept at the connection between the outer vessel flange and the inner vessel. The heat transfer rate through the inner vessel wall from the environment to the liquid helium is partially absorbed by the outer vessel and the vapor cooled screen. The heat transfer rate without any thermal intercept is

$$Q_{T_o} = -\frac{A_2}{x_c} \int_{T_o}^{T_c} \lambda(T)dT \quad (13)$$

The heat transfer rate with a thermal intercept at $T_b = 80$ K is

$$Q_{T_b} = -\frac{A_2}{x} \int_{T_a}^{T_b} \lambda(T)dT \quad Q_{T_c} = -\frac{A_2}{l - x} \int_{T_b}^{T_c} \lambda(T)dT \quad (14)$$

where $x = x_b - x_a$, $l = x_c - x_a$, and T_c is 4.2 K. The reduction of the heat leakage by the thermal intercept is from the consumption of the cooling medium on the vapor cooled screen. According to the energy conservation, there is an optimal value of x. The optimal position b can be defined by minimizing the power required to dissipate the heat leakage taking into account Carnot efficiency. The ideal Carnot cycle efficiency is

$$\eta = \frac{\dot{Q}}{W} = \frac{T_C}{T_W - T_C} \quad (15)$$

where $\dot{Q}$ is the absorbed heat, T_C and T_W are the temperatures of the cold source and the environment respectively. W is required power for refrigerator to dissipate $\dot{Q}$ and can be expressed as

Table 2
Experimental data.

	Gas outlet temperature	Position a temperature	Liquid helium temperature	Dewar pressure	Gas outlet flow	Liquid level height
Value	220 K	282 K	4.2 K	96210 Pa	3.95×10^{-5} kg/s	2100 mm

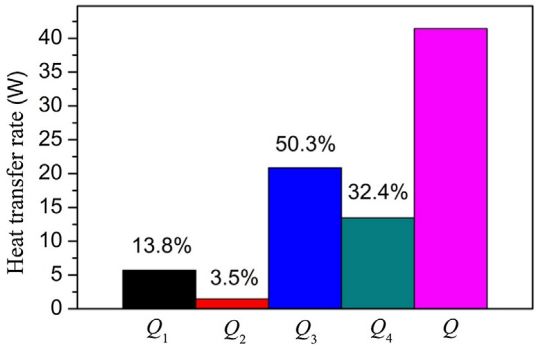

Fig. 4. Heat leakage and proportion of each part.

$$W = W_{T_b} + W_{T_c} = \frac{T_o - T_b}{T_b}\dot{Q}_{T_b} + \frac{T_o - T_c}{T_c}\dot{Q}_{T_c} \tag{16}$$

Bring in known parameters, Eq. (13) can be written as

$$W\left(\frac{x}{l}\right) = \frac{20.08}{\frac{x}{l}} + \frac{74.14}{1 - \frac{x}{l}} \tag{17}$$

According to Eq. (17), take (x/l) as the variable to draw the diagram as shown in Fig. 5. It reflects the change of required power with the thermal intercept position (Position b). The required power decreases with the downward movement of position b (vapor cooled shield height reduction) first and then rises. In other words, there is an optimal position b to minimize the power required to dissipate the $\dot{Q}$. The derivative of Eq. (17) with respect to (x/l) is as follows

$$\frac{dW}{d\left(\frac{x}{l}\right)} = -20.8\left(\frac{x}{l}\right)^2 + 74.14\left(1 - \frac{x}{l}\right)^2 \tag{18}$$

If $dW/d(x/l)$ is equal to zero, (x/l) is 0.34 (the corresponding x is 0.85 m) and the minimum value of the required power is 171.39 W. The required power without any thermal intercept is 490 W. It can be seen that the required power drops by 65% when there is a thermal intercept. So the thermal intercept plays a positive role in the reduction of the power consumption.

4.4. Effect of thermal intercept position on heat leakage

Although there is an optimal position of the thermal intercept to minimize energy consumption, the influence of the thermal intercept position on the overall heat leakage of the cryostat cannot be ignored. It can be seen from the heat transfer model established above that the thermal intercept position mainly affects the heat transfer rate Q_4 through the insulation jacket. Fig. 6 shows the variation of the heat transfer rate Q_4 with thermal intercept position. $Q_{4.1}$, $Q_{4.2}$ and $Q_{4.3}$ correspond to the three terms on the right side of Eq. (4), respectively.

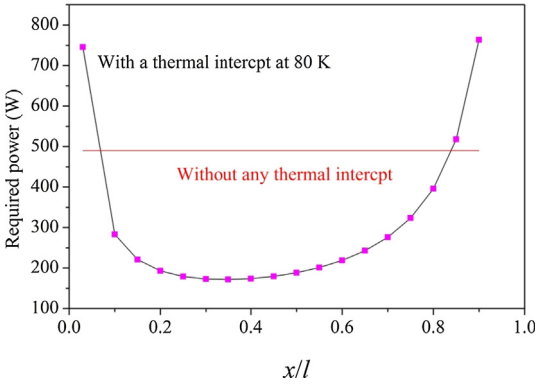

Fig. 5. Required power variation with the thermal intercept position.

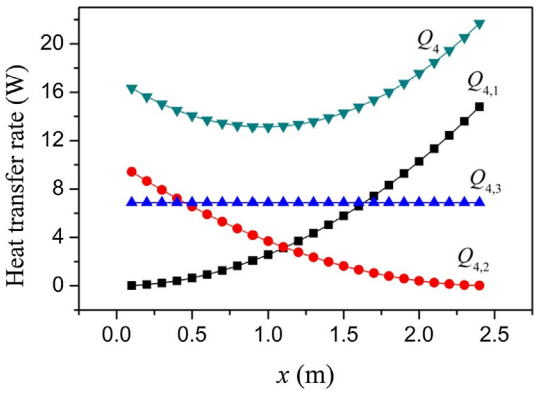

Fig. 6. Heat transfer rate variation with the thermal intercept position.

When x changes from 0 to 2.5 m, the thermal intercept position gradually moves down to the liquid level from the connection between the outer vessel flange and inner vessel wall (position a). With the increase of x, $Q_{4.1}$ goes slowly up due to enlarging of the heat transfer surface, on the contrary $Q_{4.2}$ gradually decreases, and $Q_{4.3}$ basically maintains a constant value. The heat transfer rate Q_4 which is the sum of the three parts declines first and then rises as x increases. At x = 0.97 m, Q_4 has a minimum value of 13.13 W, and $Q_{4.1}$, $Q_{4.2}$ and $Q_{4.3}$ are 2.42 W, 3.83 W and 6.88 W, respectively. From the above analysis about the thermal intercept position, it is found that when x is 0.85 m, the required power is the smallest. Therefore, based on the minimizing of heat leakage and required power, the variation of the work with x between 0.85 m and 0.97 m is plotted as shown in Fig. 7. For Q_4, the work means the required power for refrigerator to dissipate the difference from the minimum heat leakage (0.97 m, 13.13 W). For W, the work is the difference from the minimum required power (0.85 m, 171.39 W). From 0.85 m to 0.97 m, the work for Q_4 shows a downward trend and the work for W is just the opposite. It can be seen from the sum of the two parts that when x is 0.94 m, the work is the smallest, which is 1.14 W.

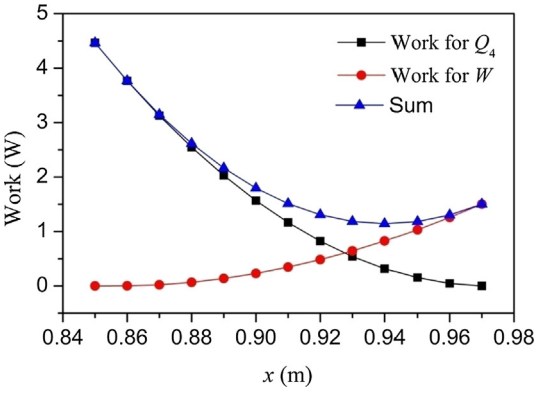

Fig. 7. Work variation with the thermal intercept position.

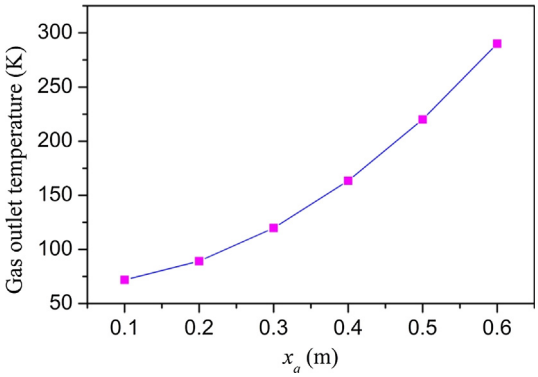

Fig. 8. Gas outlet temperature variation with height of the uninsulated part.

4.5. Height of the uninsulated part of the inner vessel

Frosting is a phenomenon that must be considered for the cryostat. The gas outlet temperature of the SCVT cryostat is a main factor affecting frost formation. For the SCVT cryostat, in order to raise the gas outlet temperature, an uninsulated part of the inner vessel is exposed to the environment. Fig. 8 shows the gas outlet temperature variation with height (x_a) of the uninsulated part. When the height changes from 0.1 m to 0.6 m, the gas outlet temperature rises from 71.83 K to 290 K. Unfortunately, the increase of the height causes the gas outlet temperature to rise and also increases the heat leakage. The heat transfer rate variation with the height is shown in Fig. 9. The total heat transfer rate Q increases with the uninsulated height and the main contributor for the increase is the change in Q_3. Therefore, although the heat leakage increases greatly, it is mainly used to heat the outlet gas, which has less influence on the liquid helium evaporation.

4.6. Liquid level height

Due to the requirements of the superconducting cavity cooling and the limitations of the SCVT cryostat, the liquid level is limited to a value between 1.8 m and 2.4 m. Fig. 10 shows the gas outlet temperature variation with the liquid level height. It can be seen from the Fig. 10, although the temperature has decreased by 29.6 K from 1.8 m to 2.4 m, maintaining a low liquid level is conducive to increasing the gas outlet temperature. The heat transfer rates variations with the liquid level height are shown in Fig. 11. When the liquid level height changes from 1.8 m to 2.4 m, the total heat transfer rate Q increases by 0.7 W. The main reason for the increase is the rise of Q_4.

5. Conclusions

In this paper, a heat leakage model is presented to investigate some

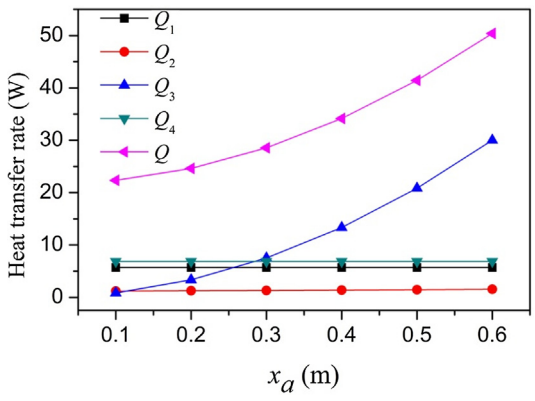

Fig. 9. Heat transfer rate variation with height of the uninsulated part.

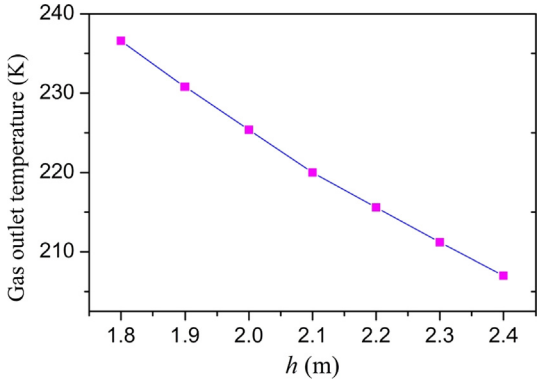

Fig. 10. Gas outlet temperature variation with the liquid level height.

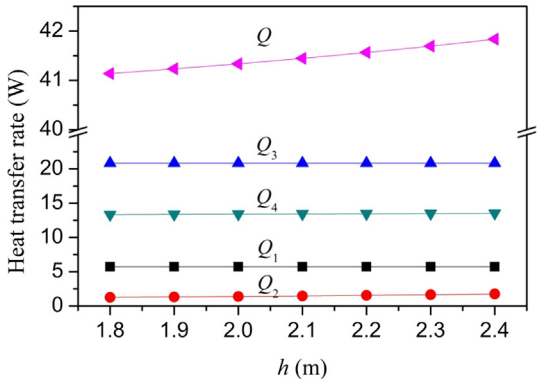

Fig. 11. Heat transfer rate variation with the liquid level height.

factors that influences the heat leakage and gas outlet temperature of the SCVT cryostat, and the model was verified by experiment. Those factors include thermal intercept position, height of the uninsulated part of the inner vessel, and liquid level height. For the SCVT cryostat studied in this paper the following results were obtained.

(1) The heat leakage obtained by experiment and heat leakage model was 45.05 W and 41.45 W, respectively. The error between the two is 8%, the model can be considered reasonable. The heat transfers through the uninsulated part of the inner vessel and insulation jacket account for the main part of the heat leakage, and the proportion are 50.3% and 32.4%, respectively.

(2) According to minimizing the power required to dissipate the heat leakage taking into account Carnot efficiency, an optimal thermal intercept position was obtained. The required power decreases with the downward movement of the thermal intercept position first and then rises. The optimal position is at 0.85 m (0.34 times the height of insulation part of the inner vessel) and has the minimum required power of 171.39 W. The required power is 490 W without any thermal intercept and drops by 65% when there is a thermal intercept. So the thermal intercept plays a positive role in the reduction of the power consumption.

(3) As the thermal intercept position changes from 0 to 2.5 m, the heat leakage reduces first and then rises. At the thermal intercept position of 0.97 m, the heat leakage though the insulation jacket has a minimum value of 13.13 W. Considering the minimum heat leakage and required power, the thermal intercept position of 0.94 m is optimal.

(4) As height of the uninsulated part of the inner vessel changes from 0.1 m to 0.6 m, the gas outlet temperature rises from 71.83 K to 290 K. Although the heat leakage increases greatly with rising height, it is mainly used to heat the outlet gas, which has less influence on the liquid helium evaporation. With a liquid level height

from 1.8 m to 2.4 m, the gas outlet temperature has decreased by 29.6 K, and the heat leakage increases by 0.7 W. So the heat leakage and gas outlet temperature is not sensitive to the liquid level height.

(5) For the SCVT cryostat studied, the optimized height of the uninsulated part of the inner vessel is 0.6 m to prevent frost formation, and the optimum distance from the flange of the outer vessel to the vapor cooled screen is 0.94 m with minimal heat leakage and minimum required power. The results provided the basis for SCVT cryostat design.

Declaration of Competing Interest

We declare that we do not have any commercial or associative interest that represents a conflict of interest in connection with the work submitted.

Acknowledgement

The authors are indebted to Department of Low Temperature, Institute of Modern Physics for providing the necessary facilities for carrying out the research work. I would also like to thank Chinese Academy of Science for providing financial support under the ADS programme (Project No. XDA03020000).

References

[1] Kim SH, Afanador R, Barnhart DL, et al. Overview of ten-year operation of the superconducting linear accelerator at the spallation neutron source. Nucl Instrum Methods Phys Res, Sect A 2017;852:20–32.
[2] Gupta PK, Rabehl R. Numerical modeling of a 2 K J-T heat exchanger used in fermilab vertical test stand VTS-1. Cryogenics 2014;62:31–6.
[3] Pierini P, Bertucci M, Maiano CG, et al. Fabrication and vertical test experience of the European X-ray free electron laser 3.9 GHz superconducting cavities. Phys Rev Accel Beams 2017;20(4).
[4] Wang GR, Chen SP, Zhang CY, et al. Heat leakage analysis and experiment research of cryogenic vessel petro-chemical. Equipment 2007;36:20–2.
[5] Xiao ZH, Wang RS, Shi YM, et al. Theoretical analysis of heat transfer of high vacuum multilayers. Vacc Sci Technol 2004;24:113–7.
[6] Wang TG, Li YN, Yao ST, et al. Study on optimal layer density of variable density multilayer insulation. Cryo Supercond 2014;42:6–9.
[7] Wang B, Huang YH, Li P, et al. Optimization of variable density multilayer insulation for cryogenic application and experimental validation. Cryogenics 2016;80:154–63.
[8] Zheng JP, Chen LB, Cui C, et al. Experimental study on composite insulation system of spray on foam insulation and variable density multilayer insulation. Appl Therm Eng 2018;130:161–8.
[9] Huang Y, Wang B, Zhou S, et al. Modeling and experimental study on combination of foam and variable density multilayer insulation for cryogen storage. Energy 2017;123:487–98.
[10] Wang J, Zhan Y, Wei W, et al. A new cost effective composite getter for application in high-vacuum-multilayer-insulation tank. Vacuum 2016;131:44–50.
[11] Wang J, Zhan Y, Wang W, et al. Optimization and performance of highly efficient hydrogen getter applied in high vacuum multilayer insulation cryogenic tank. Vacuum 2017;149:87–92.
[12] Xie T, He YL, Tong ZX. Analysis of insulation performance of multilayer thermal insulation doped with phase change material. Int J Heat Mass Transf 2016;102:934–43.
[13] Jiang WB, Zuo ZQ, Huang YH, et al. Coupling optimization of composite insulation and vapor-cooled shield for on-orbit cryogenic storage tank. Cryogenics 2018;96:90–8.
[14] Zhao T, Chen SP, Li YN, et al. Heat transfer analysis of vapor cooled shield compounded insulation and optimization of shield's position. Cryo Supercond 2016;44:17–22.
[15] Wang GP, Liu YP, Ma Q, et al. Heat loss analysis and experimental research of vertical test dewar for SRF cavity in BEPCII. Cryo Supercond 2011;39:38–41.
[16] Ozelis JP, Carcagno R, Ginsburg CM, et al. Diagnostic instrumentation for the fermilab vertical cavity test facility. Particle accelerator conference. IEEE; 2007.
[17] Yamamoto Y, Hayano H, Kako E, et al. Cavity diagnostic system for the vertical test of the baseline SC cavity in KEK-STF. Proc SRF 2007.
[18] Weise H. Superconducting rf structures – test facilities and results. Particle accelerator conference. IEEE; 2003.